VOL. 9 NO. 4
WINTER 2020

POWDER METALLURGY REVIEW

ATOMISATION AT ARCAST

DYNAMIC IMAGE ANALYSIS & LASER DIFFRACTION

SURFACE AREA IN POWDER CHARACTERISATION

www.pm-review.com

Published by Inovar Communications Ltd

Understanding how the surface area of metal powders influences Additive Manufacturing

The surface area of particles in metal powders is affected by particle size, shape, roughness and porosity. Even spherical gas atomised metal powders exhibit surface areas much higher than suggested by their size. In this article, Dave van der Wiel, Director of Technology Development at NSL Analytical Services, discusses the topic and explains why the knowledge and use of powder surface area is a critical parameter in the metal Additive Manufacturing process.

Particle morphology affects powder-based Additive Manufacturing in several ways. During powder handling, for example, the surface area of a powder strongly impacts the uptake of ambient moisture and subsequent oxidation. On the build plate, particle morphology affects the flowability, spreadability and packing of powder. Particle surface area also affects interactions between metals and binders, and strongly impacts sintering kinetics. High-temperature reactions with oxygen and nitrogen on powder surfaces during sintering and reuse are also influenced by particle morphology.

To visualise the significance of the surface area of a metal powder, consider a 30 µm iron powder with a specific surface area of 0.63 m^2/g. One hundred grams of this powder would have a surface area of 63 m^2 – nearly the area of a racquetball court. Smooth iron spheres of this size provide only 4% as much surface area, about 2.6 m^2. Fig. 1 shows where particle surface area fits uniquely into a comprehensive powder characterisation matrix, as a particle-scale morphological property (particle shape and surface texture).

Contributors to surface area in particles

For low-porosity materials, the total external (accessible) surface area of a particle is primarily a function of particle size. The 'geometric surface

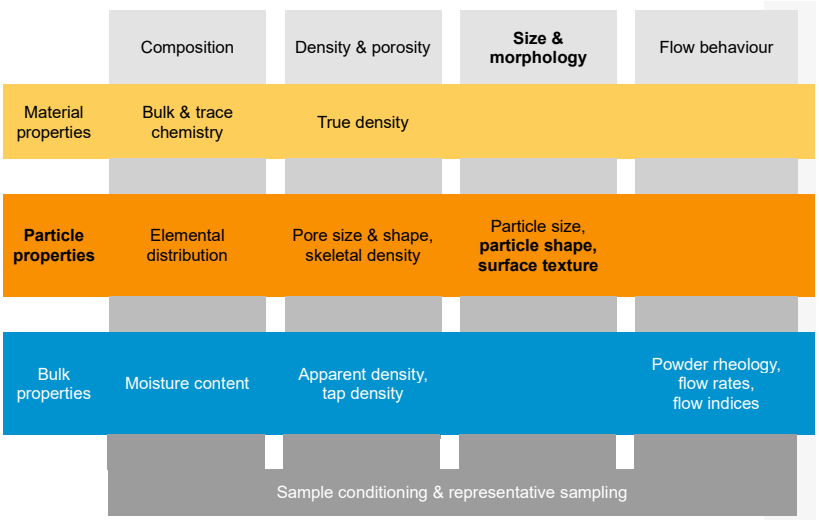

Fig. 1 Particle morphology properties associated with specific surface area

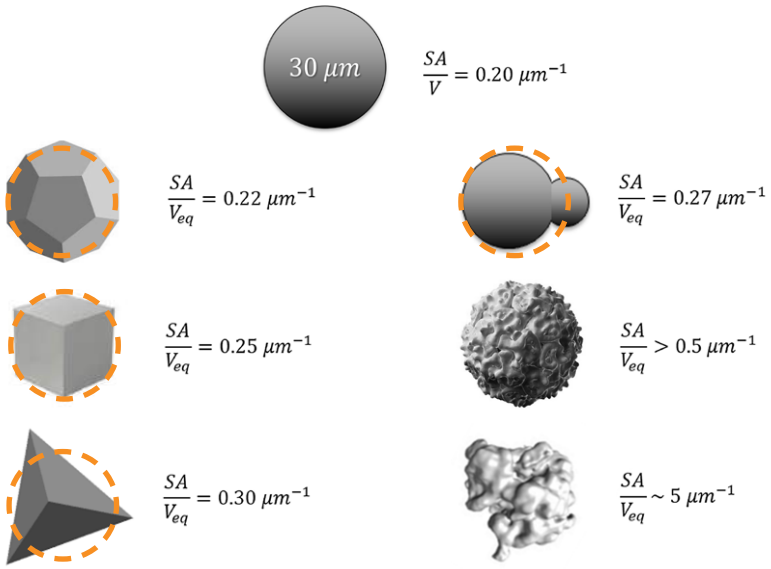

Fig. 2 Impact of particle morphology on surface area; the lower right object represents a water atomised iron particle with a surface area of 0.63 m^2/g

area' of a particle can be calculated from its median diameter, assuming perfect sphericity. A 30 μm sphere has a geometric surface area of 2,803 μm^2 and a surface area-to-volume ratio of 3/r, or 0.20 μm^{-1}.

The surface area of a powder can therefore be roughly approximated from a particle size distribution measurement. However, as shown in Fig. 2, for a given equivalent diameter, the actual surface area of real particles is strongly affected by particle shape, agglomerates, porosity and texture. For the previously mentioned 30 μm iron powder with a specific surface area of 0.63 m^2/g, the surface area-to-volume ratio is 4.9 μm^{-1} – twenty-five times greater than the smooth sphere case.

Particle morphology parameters & measurements

ISO 9276-6 provides a comprehensive list of particle shape parameters, both qualitative and quantitative [2]. These and similar morphological parameters can be grouped according to their type and scale, as shown in Table 1.

Macroshape parameters such as particle elongation are assumed to be three-dimensional and their impact on surface area is estimated based on various types of equivalent dimensions or volumes. Mesoshape parameters such as particle circularity are based on two-dimension 'shadows' of particle images (or size modes) and are estimated using equivalent areas or perimeters, for example. Surface texture is represented by parameters such as roughness factors, and (when possible) is calculated using various geometric calculations.

The techniques used to analyse for these parameters include optical image analysis, microscopy, tomography and light scattering. Some of these techniques have the advantage of simultaneously providing particle size data. The primary disadvantage of these methods is that they are indirect (and two-dimensional) estimates of three-dimensional morphologies, and either only sample 10s to 100s of particles at a time or have a limited meso/micro-scale resolution. In contrast, gas adsorption techniques provide true three-dimensional physical measurements of surface area on 10^5 to 10^7 particles.

Although particle surface area can be estimated from size and/or shape parameters, this approach does not account for microstructural features. It has been shown, for example, that even spherical gas atomised metal powders exhibit measured specific surface areas 1.8 x higher than those estimated based on particle size data [1].

Parameter scale	Particle		Surface/texture	
	"Macroshape"	"Mesoshape"	Meso	Macro to micro
Parameters	Sphericity, elongation	Circularity, angularity	Roughness factor	Surface area
Nature	3D	2D	2D	3D
Basis	Equivalent dimensions or volume	Equivalent area or perimeter Fractal analysis	Geometric or fractal analysis	Physical measurement
Techniques	Digital imaging, microscopy, tomography, laser scattering			Gas adsorption (BET)
Particles analysed	> 10 to > 100 for static microscopy > 1,000,000 for dynamic digital imaging			100,000s to 10,000,000s

Table 1 Particle morphology types, scales and measurement

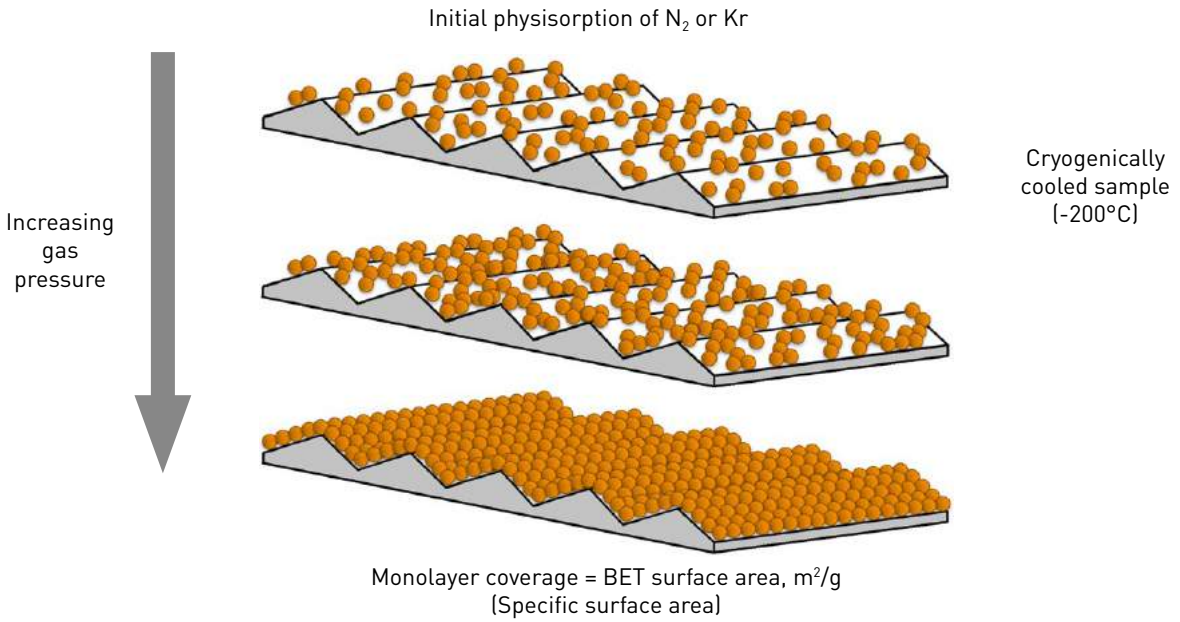

Fig. 3 Measurement of specific surface area by gas adsorption

BET surface area of metal particles

The same van der Waals forces that are responsible for particle-to-particle adhesion in < 100 µm powders also lead to the adsorption of gases on solid surfaces. This phenomenon is used to quantitatively measure the surface area of solid surfaces using the well-known BET method [3, 4].

This method involves cooling a sample to cryogenic temperatures, followed by stepwise introduction of an adsorbate gas (Fig. 3). Liquid nitrogen (77K) is used as the cryogenic medium for convenience. The equilibrium pressure after each successive gas dose generates an adsorption isotherm until monolayer coverage is reached. A model is applied to the adsorption data to provide the specific surface area, expressed in m^2/g (or m^2/kg).

For materials with surface areas of less than about 1 m^2/g, it is necessary to use krypton gas as the adsorbent instead of the more common adsorbate nitrogen. The lower saturation vapour pressure of liquid Kr at 77K (350 Pa compared to 101 kPa for N_2) reduces the amount of dead volume gas by a factor of about 300, thus increasing the magnitude (and therefore the resolution) of the pressure differentials used for the BET method. Krypton is therefore recommended for low surface area materials by IUPAC [5], ISO [6] and ASTM [7].

Relevant BET gas adsorption test standards include ISO 9277 [6], ASTM B922 [8] for metal powders and ASTM D4780 [7]. Although the latter standard applies to ceramics, it is specific to krypton adsorption for low surface area materials. Luk provides a review of the measurement and calculation of the surface area of metal powders, including a thorough review of the BET gas adsorption method [9].

Badalyan & Pendleton conducted a rigorous analysis of the propagation of uncertainty in N_2 BET measurements, estimating a relative combined uncertainty of ±0.63% [10]. More recently, the ASTM B09 committee conducted an interlaboratory study for test method B922, which included both N_2 and Kr BET measurements from five laboratories [11]. The materials used in this study included stainless steel and tungsten powders with surface area values from 0.140 to 0.546 m^2/g. The relative standard deviation values for repeatability in this study range from 1.6–11.4%.

Unsurprisingly, all these studies report diminished precision as surface area value decreases. The BAM reference procedure for gas adsorption reports an uncertainty of ± 10% for a 0.1 m^2/g material [12]. However, to the author's knowledge, no such studies have been conducted on metal powders exclusively using krypton gas as a sole adsorbate.

Micromeretics provides approximations of the maximum uncertainty for a range of total sample surface areas using either N_2 or Kr gas (Table 2) [13]. As can be seen, only Kr provides acceptable uncertainties for the measurement of low surface area materials.

Examples of variations in surface area due to metal particle morphology

Table 3 lists some properties of three similarly-sized commercial iron powders produced by Höganäs AB. The different production methods used for these powders are known to result in substantially different particle morphologies.

The particle size distribution for these powders is quite similar, ranging from about 20 µm to 180 µm, with 18% to 23% less than 45 µm,

Total sample area (m^2)	Maximum uncertainty	
	N_2	Kr
10	2.4 to 6.7%	0.20%
5	4.7 to 13%	0.31%
2	12 to 34%	0.77%
1	24 to 67%	1.5%
0.5		3.1%
0.2		7.7%

Table 2 Maximum uncertainty in BET surface area for N_2 and Kr adsorption (Micromeretics [13])

resulting in median diameters that vary by only about 2%. The porosity and shape differences of these powders produce about 4–5% variation in their densities. Yet the measured specific surface areas differ by 40%, providing clear quantification of the morphological differences between these powders.

The correlation of powder-specific surface area and particle morphology has been described by many authors, including Unal *et al.*, who studied the impacts of gas atomising conditions on ca. 35 µm aluminium powders using both BET surface area and electron microscopy (Table 4) [14, 15]. The authors demonstrated that specific surface area values below 200 m^2/kg corresponded to spherical particles, 255 to 306 m^2/kg to globular or elongated particles and 302 to 316 m^2/kg to angular particles. Obviously, the BET surface area data has the advantage of being quantitative, more representative and easier to gather.

Application to Additive Manufacturing

Water atomised powders commonly used in conventional Powder Metallurgy processes can have irregularly shaped particles with relatively high surface area. Air- and inert gas atomised powders were initially developed for oxygen-sensitive materials like aluminium and titanium. The high sphericity of gas atomised powders improves handling for use in Additive Manufacturing, but provides much lower surface area (Table 5 [16]). The larger particle size ranges used in AM processes also provide less surface area compared to conventional PM processes.

	Sponge iron		Atomised iron	
	NC100.24	SC100.26	ASC100.29	Variation
d50 (µm)	87	85	84	**±1.5%**
Apparent density (g/cm^3)	2.45	2.7	2.8	±4.7%
Tap density (g/cm^3)	3.2	3.5	3.5	±4.2%
Surface area (m^2/kg)	60	40	20	**±41%**

Table 3 Variation in surface area of three similarly sized iron powders

Sintering of particles is driven by the excess free surface energy associated with their relative high surface area, and many studies have shown the improvements in densification resulting from the addition of higher surface area metals powders to lower surface area spherical powders (Table 6 [17])

Depending on the material and AM process used, powder surface area may be optimal at either higher or lower levels.

Lower surface area:

- Decreases the reactivity of metals such as titanium, aluminium, etc.
- Decreases sensitivity of product powders towards ambient moisture

While higher surface area:

- Promotes sintering and densification – potentially offsetting lower green densities
- Improves interactions between metals and binders.

Other considerations related to powder surface area include the fact that the focus of cost reductions in many AM processes is shifting from equipment to raw materials, and inert gas atomised powders can be ten times more expensive than their water atomised analogs. In addition, highly spherical powders may not be necessary in all powder bed processes, and powder recycling can drive toward less-reactive morphologies.

These factors, along with the use of H_2 sintering to remove oxygen, have increased interest in the use of water atomised powders in some AM processes [18–21]. Similarly, the use of non-spherical powders from Hydride-Dehydride (HDH) processes is seeing increased application to AM [22, 23].

Zhou studied the densification of stainless steel 420 specimens produced by binder jet Additive Manufacturing (BJT) using 30 µm water and gas atomised powders [24, 25]. This work employed fractal analysis of electron micrographs to describe the particle morphology; for a description of fractal dimension, see Klobes 2006 [4].

As applied by Zhou to micrographs at 1000 x magnification, the fractal

Powder type	Atomisation gas	Median particle diameter (µm)		Surface area (m^2/kg)	SEM morphology
Al	21% O_2	42.1	Avrg 33.6	**316**	**Angular**
	12% O_2	25.0		**302**	
	6% O_2	33.1	Avrg 33.9	**306**	**Elongated**
	N_2 – 5% O_2	34.7		**290**	
	3% O_2	33.1	Avrg 34.6	**287**	**Globular**
	N_2 - 3% O_2	36.0		**255**	
	2% O_2	31.9	Avrg 34.3	**187**	**Spherical**
	1% O_2	34.8		**151**	
	N_2 – 0.5% O_2	35.8		**133**	
	N_2	34.5		**135**	
AlCuMgSi	N_2	31.9	Avrg 33.7	**139**	**Spherical**
	Ar	31.9		**137**	
	Ar	37.1		**119**	

Table 4 Correlation between particle morphology and surface area for gas atomised aluminium powders [14,15]

dimension would be included as a 'mesoshape' parameter in Table 1. One would therefore expect fractal dimension to vary in proportion to surface area, but with considerably less sensitivity since it neglects microtextural effects; in fact, Jiqiao & Baiyun showed that BET surface area variations on tungsten powders were about 10 x greater than fractal dimension [26]. Table 7 shows the sintered porosity and densification of two representative specimens which employed the two powder types, with each powder's fractal dimension indicated [24, 25]. As can be seen, the less uniform water atomised powder produced lower porosity and higher densification at a given sintering condition. Fig. 4 (adapted from Zhou) demonstrates both increased kinetics and extent of sintering with the higher surface area powder.

Similarly, Hoeges *et al.* studied Laser Beam Powder Bed Fusion (PBF-LB) of water and gas atomised 316L powders [27], and Nomura *et al.* have reported on the mechanical performance of cobalt alloy specimens produced by PBF of water and gas atomised powders [28]. In these cases too, specimens produced from higher surface area water atomised

Particle size, d50	17-4PH Powder surface area	
	Gas atomised	Water atomised
6.5 – 8.0 µm	0.31 m^2/g	0.36 m^2/g
10 – 11 µm	0.23 m^2/g	0.34 m^2/g
19 – 20 µm	0.15 m^2/g	0.22 m^2/g

+50%

Table 5 Comparison of surface areas of gas and water atomised powders [16]

Powder fractions		Sintered specimens	
Water atomised (203 m^2/kg)	Gas atomised (89 m^2/kg)	Density (g/cm^3)	Porosity (%)
0%	100%	7.36	7.94
25%	75%	7.43	7.12
50%	50%	7.56	5.44
75%	25%	7.60	5.00
100%	0%	7.61	4.87

Table 6 Density and porosity of sintered 316L as a function of powder surface area [17]

Powder (30-µm)		Sintered specimen	
Type	Fractal dimension	Porosity	Densification
Water atomised	1.70	3.9%	90%
Gas atomised	1.03	9.1%	70%

Table 7 Impact of particle morphology on powder-bed printed stainless steel 420 [24, 25]

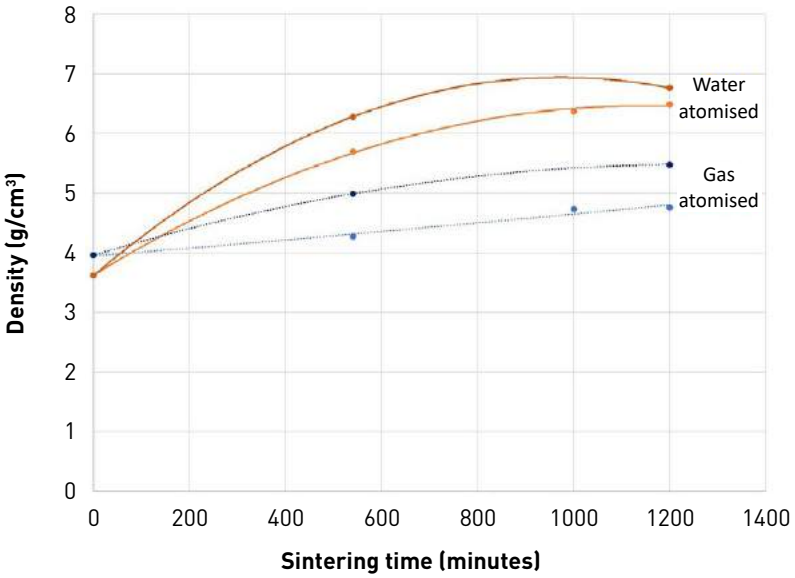

Fig. 4 Kinetics and extent of powder-bed sintering of two stainless steel 420 powders (adapted from [24,25])

powders were capable of producing physical and/or mechanical properties that were comparable or better than low surface area gas atomised powders. The authors in both studies indicated that the improved sintering of the high surface area powders offsets disadvantages of lower flowability and/or green densities.

Summary

Metal particle surface area measurements by krypton gas adsorption provide direct measurement of multi-scale, three-dimensional particle morphology on samples comprising millions of particles. As such, they represent a unique facet of powder characterisation that is not represented by direct estimates of two-dimensional particle representations.

The dramatic impact of particle surface area on sintering processes is well-known and has been shown to offset challenges in powder handling where non-spherical powders are employed in AM processes. Thus, with raw material costs and powder reuse an increasing concern, the knowledge and use of powder surface area has re-emerged as a critical parameter in metal Additive Manufacturing.

Author

Dave van der Wiel
Director of Technology Development
NSL Analytical Services
4450 Cranwood Parkway,
Cleveland, Ohio 44128, USA
dvanderwiel@nslanalytical.com
www.nslanalytical.com

References

[1] Schrøder-Pedersen, A., *et al.*, J. Test. Eval. 25(4), 365 (1997).

[2] ISO 9276-6, Descriptive and quantitative representation of particle shape and morphology, 2008.

[3] Brunauer, Emmett and Teller, *J. Am. Chem. Soc.* 60(2), 309 (1938).

[4] Klobes, P., *et al.*, NIST Special Publication 960-17, 2006.

[5] Thommes, M., *et al.*, *Pure Appl. Chem.* 87(9-10), 1051 (2015).

[6] ISO 9277, Specific Surface Area of Solids by Gas Adsorption Using the BET Method, 2010.

[7] ASTM D4780, Low Surface Area of Catalysts and Catalyst Carriers by Multipoint Kr Adsorption, 2017.

[8] ASTM B922, Metal Powder Specific Surface Area by Physical Adsorption, 2020.

[9] Luk, S., ASM Handbook Vol. 7, Powder Metallurgy, P. Samal and J. Newkirk (eds.), ASM International, 2015.

[10] Badalyan, A. and P. Pendleton, Langmuir 19(19), 7919 (2003).

[11] ASTM Research Report RR:B09-1026, ASTM International (in press).

[12] BAM Reference Procedure 402, Precision Measurement of the Specific Surface Area of Solids by Gas Adsorption, 2016.

[13] Micromeretics, Tech Tip 14, retrieved from www.micromeritics.com

[14] Ozbilen, S., A. Unal and T. Sheppard, Physical Chemistry of Powder Metals: Production and Processing, W.M. Small (ed.), The Minerals, Metals & Materials Society, 489, 1989.

[15] Unal, A., *Powder Metall.* 32(1), 31 (1989).

[16] Hausnerova, B., *et al.*, *Powder Technol.* 312, 152 (2017).

[17] Bonato, M., *et al.*, *Mater. Sci. Forum* 498-499, 164 (2005).

[18] Hoeges, S., *et al.*, *Met. Powder Rep.* 72(2), 111 (2017).

[19] Letenneur, M., *et al.*, *J. Manuf. Mater. Process.* 1(2), 23 (2017).

[20] Durejko, T., *et al.*, *Materials* 11(5), 843 (2018).

[21] Fedina, T., *et al.*, Addit. Manuf., in press (2020).

[22] Xu, W., *et al.*, *J. Mater. Sci. Technol.* 35(2), 322 (2019).

[23] Narra, S., *et al.*, Addit. Manuf. 34, 101188 (2020).

[24] Zhou, Y., *et al.*, Proceedings of MS&T 2014, Oct 12-16, Pittsburgh, PA (2014).

[25] Zhou, Y., Master's Thesis, Univ. Pittsburgh, 2014.

[26] Jiqiao, L. and H. Baiyun, *Int. J. Refract. Met. Hard Mater.* 19, 89 (2001).

[27] Hoeges, S., *et al.*, World PM2016, in Whittaker, D., *Metal AM* 3(1), 101 (2017).

[28] Nomura, N., *et al.*, World PM2016, in Whittaker, D., *Metal AM* 3(1), 101 (2017).